Erythropoietin directly affects single hematopoietic stem cell differentiation after transplantation

A.S. Eisele, J. Cosgrove, Aurélie Magniez, E. Tubeuf, S. Tenreiro Bento, F. Cayrac, T. Tak, A.M. Lyne, J. Urbanus, L. Perié

Erythropoietin directly affects single hematopoietic stem cell differentiation after transplantation

A.S. Eisele[1,2], J. Cosgrove[1,2], A. Magniez[1,2], E. Tubeuf[1,2], S. Tenreiro Bento[1,2], F. Cayrac[1,2], T. Tak[1,2], A.M. Lyne[1,2], J. Urbanus[3] and L. Perié[1,2*].

Affiliations

1. Institut Curie, PSL Research University, CNRS UMR168, Paris, France.
2. Sorbonne Universités, UPMC Univ Paris 06, France
3. Netherlands Cancer Institute, Amsterdam, Netherlands

Contact information

Leila.Perie@curie.fr

Abstract

The cytokine erythropoietin (EPO) is a potent inducer of erythrocyte development and one of the most prescribed biopharmaceuticals. The action of EPO on erythroid progenitor cells is well established, but its action on hematopoietic stem cells (HSCs) is still debated. Here, using cellular barcoding, we traced the differentiation of hundreds of single HSCs, after *in vitro* EPO exposure and transplantation, in five different hematopoietic cell lineages, and observed the occurrence of high-output Myeloid-Erythroid-megaKaryocyte (MEK)-biased and Myeloid-B-cell-Dendritic cell (MBDC)-biased clones. ScRNAseq analysis of *in vitro* EPO-exposed HSCs revealed upregulation of erythroid associated genes in a subset of HSCs. Collectively, as well as demonstrating a direct effect of EPO on HSCs, our results suggest an EPO-mediated induction of MEK-bias in multi-outcome HSCs, and that this change in output is functionally compensated by MBDC-biased HSCs.

Introduction

Erythrocytes are the most numerous hematopoietic cells in our body and are constantly renewed[1]. The major inducer of erythroid cell development in steady state and during anemic conditions is the cytokine EPO[2]. Recombinant EPO is widely used to treat anemia and is one of the most sold biopharmaceuticals[3]. Previously, EPO was thought to solely target erythroid-committed progenitors and induce their increased proliferation and survival via the EPO receptor (EPOR)[4]. Recently, alternative EPO receptors (EphB4[5], CD131[6], and CRFL3[7]) have been described, opening new pathways for EPO action. EPO has been shown to also target hematopoietic niche cells (osteoblasts and osteocytes[8,9], endothelial cells[10,9], adipocytes[11,12], mesenchymal stem cells[13,14]). In the hematopoietic hierarchy, EPO has also been

suggested to act on hematopoietic stem and progenitor cells[15,13,16,17,18,19,20,21], but several aspects remain debated.

First, it is unclear through which receptor EPO could act on HSCs. Both transcription[22,23,24,25,13], and no transcription[9] of *Epor* have been reported in HSCs, as well as EPOR surface expression on HSCs[13,26] and the expression of alternative EPO receptors (EphB4[27,28,29], CD131 and CRFL3[23]). Secondly, different effects of EPO on HSCs have been observed. In early studies, high EPO levels were associated with increased HSC proliferation[15,21]. More recently, upregulation of cell cycle-related genes in HSCs following an increase of EPO levels *in vivo* corroborated these findings[17,18,20]. In addition, an increased EPO level was found to impact expression of immune response genes[18] or bone homeostasis-associated genes[13] in HSCs. In parallel, the upregulation of erythroid genes in HSCs in response to EPO[20,16], as well as an increased erythroid production and decreased myeloid cell production after transplantation of *in vivo* EPO-exposed HSCs[16], has been observed. Others, however, reported that multi-potent progenitor subsets, rather than HSCs, change cell cycle- and lineage-associated gene expressions after *in vivo* EPO exposure [18,19]. In summary, the findings on the effect of EPO on HSCs are conflicting.

For a long time, the mechanism of cytokine action on HSCs has been an important research topic[30,31,32,33,34,35]. One difficulty is the discrimination between direct effects of cytokines on HSCs and indirect effects through action on the HSC environment[36]. It is now established that HSCs are heterogenous in the quantity (lineage-bias) and the type of cells (lineage-restriction) they produce, and myeloid-, lymphoid-, and platelet or platelet/erythroid-biased and restricted HSCs as well as lineage-balanced HSCs have been described[37,38,39,40,41,42,43,44]. Cytokines have been reported to act directly on the lineage production of the heterogenous pool of HSCs

through the selective proliferation or survival of pre-existing lineage-biased HSCs[45,46] or through *de novo* lineage instruction of HSCs[47,48]. In addition indirect effects of cytokines on HSCs have been reported[36]. Only a clonal assessment of single HSCs using methods to trace the fate of single HSCs can distinguish these direct actions of cytokines.

For the cytokine EPO, evidence for the selective proliferation of pre-existing lineage-biased HSCs and *de novo* lineage instruction of HSCs is still lacking. Importantly, as most studies analyzed the effect of *in vivo* EPO exposure on HSCs[8,9,10,11,12,13,14], it is still unclear whether EPO acts directly on HSCs, via their environment, or both. To address the direct effects of EPO on HSC differentiation after transplantation at the clonal level, we here utilize cellular barcoding technology which allows us tracing of the progeny of hundreds of single HSCs *in vivo*. By analyzing cellular barcodes in five mature hematopoietic lineages and the HSC compartment, we observed high-output MEK-biased and MBDC-biased HSC barcode clones after EPO-exposure. ScRNAseq of *in vitro* EPO-exposed HSCs revealed upregulation of erythroid associated genes in a subset of HSCs. Our results demonstrate a direct effect of EPO on HSC differentiation after transplantation with implications for basic HSC research and therapeutic applications in the clinic.

Results

Effect of EPO-exposure on HSC biases four weeks after transplantation. To study the effect of *in vitro* EPO exposure on HSC differentiation after transplantation, we labelled sorted HSCs (C-Kit$^+$ Sca1$^+$ Flt3$^-$ CD150$^+$) (Supplementary Fig. 1a) with a unique genetic barcode as previously described[49], exposed them to EPO (1,000 ng/ml)

or PBS for 16 hours *in vitro* and transplanted them into 6 Gy sub-lethally irradiated recipient mice (Fig. 1a). We used a newly generated lentiviral barcode library (LG2.2) with high diversity (18,026 barcodes in reference list), consisting of random 20 nucleotides sequences positioned adjacent to the green fluorescent protein (GFP) gene. At day 30 after transplantation, barcoded (GFP^+) erythroblasts (E; $Ter119^+$ $CD44^+$), myeloid cells (M; $Ter119^-$ $CD19^-$ $CD11c^-$ $CD11b^+$), and B-cells (B; $Ter119^-$ $CD19^+$) (Supplementary Fig. 1b-c, e) were sorted from the spleen and their barcode identity assessed through PCR and deep-sequencing. No difference in chimerism was observed between the EPO and control group in the spleen and blood, even when mTdTomato/mGFP donor mice were used to better assess the erythroid lineage (Fig. 1b-c). We observed a change in the differentiation pattern of HSCs from balanced to unbalanced pattern upon EPO treatment compared to controls, as seen in the triangle plot in which fewer HSCs were at the center of the triangle in the EPO group (Fig. 1e, Supplementary Fig. 2a). The number of barcodes producing each lineage was similar in both groups (Fig. 1d), indicating that EPO exposure didn't affect the number of engrafting and differentiating HSCs after transplantation. The number of erythroid restricted HSCs was not increased in the EPO group as compared to control (Fig. 1e), indicating that the response to EPO is more complex than a direct instruction of erythroid restricted HSCs. To better quantify the change in the HSC differentiation pattern upon EPO exposure, barcode-labeled HSCs were assigned to lineage-biased classes using a classifier that is based on the balance of cellular output between the M, B and E lineages. For a 10% threshold classifier, this means for example that HSCs classified as ME-biased had above 10% of their output in the M and E lineage, and under 10% of their output in the B lineage (Supplementary Fig. 2b). Interestingly, although the percentages of the different classes of lineage-biased HSCs in control

and EPO group were not significantly different (Fig. 1f), their contribution to the different lineages was modified (Fig. 1g). In the control group, balanced HSCs (MBE) produced the majority of all lineages, as previously published[50], whereas their output was reduced in the EPO group (Fig. 1g). In the EPO group, ME- and MB- biased clones produced most cells of the analyzed lineages (Fig. 1g). ME-biased HSCs produced the majority of erythroid cells (57% +/- 10%), MB-biased HSCs produced the majority of B-cells (58% +/- 36%), and ME- and MB-biased HSCs contributed the majority of myeloid cells (MB-biased 45% +/- 38% and ME-biased 20% +/- 13%, together 65% +/- 25%). To test the significance of this effect, we used a permutation test, which compares the effect size between control and EPO group to the one of all random groupings of mice[51]. The contributions of the ME- and of the MB-biased HSC classes to the different lineages were significantly different in EPO and control groups (Supplementary Table 1). These results held for different classification threshold values and were reproduced in an additional experiment (Supplementary Fig. 2c-g). Overall, EPO affected the balance in cell production of HSCs by inducing changes in the cell output of lineage-biased HSCs, but no difference in their number i.e., no difference in the clonal composition of the HSC compartment itself. One average we detected around one hundred barcodes per mouse (Fig. 1d) which gives enough power to our analysis. However, small changes in clonal composition cannot be formally excluded. We repeated the experiment with a lower EPO concentration (160 ng/ml) as well as with an additional single injection of EPO (16,000 IU/kg) during transplantation. Both setups gave similar results (Fig. 2, Supplementary Fig. 3), with significantly increased contribution of the ME-biased HSC category to the myeloid and erythroid lineages, and of the MB-biased HSC category to the B and myeloid lineage in the EPO group, as detected by permutation testing (Supplementary Table 1). In summary, *in*

vitro EPO priming of HSCs modified the output balance of HSCs rather than the clonal composition of lineage-restricted and -biased HSCs. Balanced HSCs produced a smaller percentage of the mature cells; ME-biased HSCs produced most of the erythroid cells and MB-biased HSCs produced most of the B cells.

Contribution of biased HSCs to the DC and MkP lineage after EPO exposure. To further characterize the cells produced by the ME-biased and MB-biased HSCs, we repeated our experimental set up including the analysis of the megakaryocyte and dendritic cell (DC) lineages (Fig. 3). Megakaryocyte Progenitors (MkP) were chosen as proxy for the production of platelets which are not suitable for barcode analysis. Barcoded (GFP^+) DCs (DC; Donor $Ter119^-$ $CD19^-$ $CD11c^+$ $CD11b^-$) and MkP (MkP; C-Kit^+ $Sca\text{-}1^-$ $CD150^+$ $CD41^+$) (Supplementary Fig.1 c-e) were sorted together with M, E, and B cells, 4 weeks after transplantation of control or EPO-exposed HSCs (1,000 ng/ml). In both groups, the majority of the balanced, ME-, and MB-biased HSCs produced also DCs (Fig. 3a). We observed a minor contribution of DC-restricted HSCs to the DC lineage, as previously reported[49] (Fig. 3b). In the control group, balanced HSCs produced the majority of DC (65% +/- 9%) (Fig. 3b). However, in the EPO group, balanced HSCs decreased their contribution to the DC lineage (36% +/-25%) and MB-biased HSC significantly increased their contribution to DC production (86% +/- 43% EPO vs 22% +/- 11% control group) (Fig. 3b). Thus, they were MBDC-biased HSCs. In contrast the ME-biased HSCs produced few DCs in both groups (Fig. 3b), indicating that ME-biased HSCs are restricted both in their B and DC production compared to the M and E production. Again, all the observed effects were significant by permutation testing (Supplementary Table 1).

The majority of the MkP production came from the ME-biased HSCs in both groups (58% +/- 21% control and 55% +/- 14% EPO group, Fig. 3c-d), indicating that ME-biased HSCs were also MkP-biased HSCs (thus MEK-biased). We did not detect a high contribution of MkP-restricted HSCs[41,40,52] to the MkP lineage (01% +/- 1% in control and 3% +/- 4% in EPO group, Fig. 3d). Finally, as high EPO exposure has been linked to changes in macrophage numbers[53], we analyzed the contribution of control and EPO-exposed HSCs to the myeloid lineage in more detail. Barcoded myeloid lineage (GFP^+ Donor $Ter119^-$ $CD19^-$ $CD11c^-$ $CD11b^+$) macrophages (Ma; $CD115^-$ $Siglec\text{-}F^-$ $Ly6G^-$), eosinophils (Eo; $CD115^-$ $Siglec\text{-}F^+$ $Ly6G^-$), monocytes (Mo; $CD115^+$ cells), and neutrophils (Neu; $CD115^-$ $Siglec\text{-}F^-$ $Ly6G^+$), were sorted together with B, and E cells as before for analysis (Supplementary Fig. 4a). We could not detect changes in the percentage of the different myeloid subsets produced by the bulk or single HSCs after transplantation in control and EPO group (Supplementary Fig. 4b-c).

ScRNAseq profile of HSCs after *in vitro* culture. One concern when studying the differentiation of *in vitro* EPO-exposed HSCs is that *in vitro* culture could alter HSC properties and already initiate differentiation. We analyzed the cell surface phenotype of the HSCs after *in vitro* culture (Supplementary Fig. 1f) and observed that the majority of cells conserved the original sorted phenotypes with a slight downregulation of c-Kit, which is known for cultures containing stem cell factor[54]. To further characterize the cells that were injected, we performed single cell RNA sequencing (scRNAseq) of barcoded HSC after the *in vitro* culture in medium supplemented with EPO or PBS using the 10X Genomics platform. 1,706 cells from control and 1,595 cells from the EPO group passed our quality control and were mapped to a published dataset to perform supervised cell type annotation. We generated a reference map of 44,802 $ckit^+$

cells from[55] and used published signatures[56,19,57] to annotate this map for ckit$^+$ cells, LSK, MPP4, lymphoid, erythrocytes, megakaryocyte and myeloid progenitors (Fig. 4a and Supplementary Fig. 5b). We then projected our single cell data on this map using k-nearest neighbors mapping[58]. We observed that both the control and the EPO-exposed HSCs similarly overlapped with non-MPP4 LSK cells, according to their sorting phenotype (C-Kit$^+$ Sca1$^+$ Flt3$^-$ CD150$^+$) (Fig. 4b). These results indicate that neither the *in vitro* culture itself nor the EPO treatment dramatically affected the identity of the sorted HSCs. To benchmark our mapping and projection method, we projected erythroid progenitors from an independent dataset[19] onto the reference map and found they mapped to the predicted region of the annotated map (Supplementary Fig. 5a). This analysis suggests that EPO-exposed HSCs retain their identity after *in vitro* culture and before transplantation.

Effect of EPO-exposure on HSC scRNAseq profile. The scRNAseq data was further analyzed using the Seurat package[59] to look for the effect of EPO exposure. When comparing the EPO and control group, we found 1,176 differentially expressed genes (Fig. 4c and Supplementary Table 2) and this number was significantly higher than the number expected due to chance (p-value=0,01) as assessed by permutation test. Among the most upregulated gene in the EPO-exposed HSCs, were genes with clear erythroid association as *Hbb-bs*, *Erdr1*, *Wtap*, *Kmt2d*, or *Nfia*[60], GATA1 targets (*Abhd2*, *Cbx3*, *Kdelr2*, *Pfas*), cell cycle related genes (*Tubb5*, *Hist1h2ap*) as well as genes previously described to be induced in HSCs after *in vivo* EPO exposure, such as *Bmp2k*[13] and *Ifitm1*[17] (Fig. 4c). Genes involved in stem cell maintenance, such as *Serpina3g*, *Mecom, Txnip*, *Meis1*, *Pdzk1ip1*[17], *Sqstm1*[61], *Smad7*[62], *Aes*[63], were among the most downregulated genes in the EPO-exposed HSCs (Fig. 4c).

As our cellular barcoding data suggests that single HSCs differ in their response to EPO, we assessed the heterogeneity of EPO responses at the transcriptomic level. UMAP-based visualization of the data suggested that a small group of EPO treated cells had a distinct transcriptomic profile from the rest of the dataset (Fig. 4d). This observation was independent of the number of PCA components and genes used in the analysis (Supplementary Fig. 5c). We then defined an EPO response signature based on the genes significantly upregulated in the EPO group compared to the control group and analyzed the expression of this signature in the EPO-exposed HSCs. The cells that were enriched in the EPO group compare to control were also expressing the highest score for the EPO response signature (Fig. 4e), indicating that the key molecular differences between our control and EPO groups were driven by a subgroup of cells. Reasoning that this subgroup contains the cells directly responding to EPO, we defined as EPO-responders, cells in the 90^{th} percentile of EPO response signature expression (Fig. 4e). Note that when cells were clustered in three groups based on the stability analysis of unsupervised clustering (Supplementary Fig. 5d-e), EPO responders were enriched in cluster 2 relative to the others (Supplementary Fig. 5f), corroborating our results from supervised analysis that EPO responders were a subgroup of EPO-exposed HSCs. The genes encoding EPOR, as well as the alternative EPO receptors EphB4, CD131, CRFL3 were equally expressed between the EPO-responders, non-responders and control groups (Supplementary Fig. 5g). Reasoning that the EPO-responders could correspond to MEK-biased HSCs, we also looked for potential MBDC-biased HSCs but could not detect a subgroup of cells with upregulation of lymphoid associated genes, suggesting that the MBDC-bias is not a direct effect of EPO exposure but more an indirect effect. In summary, *in vitro* EPO

exposure induced the upregulation of erythroid genes and downregulation of stem cell maintenance genes in a subgroup of HSCs.

Effect of EPO on HSC self-renewal. As we observed changes in stem cell maintenance-associated gene expression after *in vitro* EPO exposure, and in light of previous studies which suggested changes in HSC proliferation after *in vivo* EPO exposure[15,2117,18,20], we next explored if the self-renewal capacity of HSCs was impacted after *in vitro* EPO-exposure and transplantation. We therefore analyzed barcodes in bone marrow HSCs in addition to the spleen E, M, and B lineages at week 4 after transplantation of control and EPO-exposed HSCs (160 and 1,000 ng/ml) (Fig. 5). Most of the barcodes detected in HSCs were also present in the mature cells (Fig. 5b) and this was unchanged in the EPO group, indicating that most of the HSCs were actively differentiating at 4 weeks post-transplantation both in the control and the EPO groups. Not all barcodes detected in mature cells were also present in HSCs (Fig. 5b), indicating that these barcoded HSCs were not self-renewing or below the limit of detection. Despite confidently detecting similar numbers of barcodes in HSCs (Fig. 5a) and in the mature lineages (Fig. 1d), the limit of barcode detection does not allow to formally exclude the presence of these barcodes in a small number of HSCs.

To analyze if different HSC biases correlated to different self-renewal capacity, we analyzed the proportion of biased HSC classes as previously defined within the HSC compartement (Fig. 5c). In the control group, balanced and ME-biased HSCs contributed most to the HSC reads (34% +/- 36% MBE and 37% +/- 34% ME-biased HSCs), while barcodes of MB-biased HSCs contributed less (15% +/- 32%) (Fig. 5c), a trend that has been previously described[64,65,41]. Surprisingly, the pattern of contributions of different biased HSC subsets to HSC reads was unchanged in the

EPO groups (Fig. 5c), implying that the extent of self-renewal in different self-renewing biased HSC classes was unchanged after *in vitro* EPO exposure.

To study if the increased production of cells by the ME- and MB-biased HSCs to the mature cells observed after *in vitro* EPO-exposure (Fig. 1-3) correlated with self-renewal capacity of HSCs, we analyzed the contribution of barcodes detected or not in HSCs to the E, M, and B lineages (Fig. 5d). The majority of mature cells were derived from barcodes also present in HSCs in the control group. In both EPO groups, the contribution of barcodes detected in HSCs to mature cells was lower (Fig. 5d) and this difference was significant by permutation testing (Supplementary Table 1). These results imply that the increased contribution of biased HSC classes to the mature cell lineages after *in vitro* EPO-exposure is most likely caused by cells not detected within HSCs, and thereby cells possibly differentiating more than self-renewing. However, as stated before, the limit of barcode detection in HSCs does not allow to formally exclude the presence of these barcodes in few HSCs.

Effect of EPO-exposure four months after transplantation. Finally, to test the duration of the effect of EPO exposure on HSCs, we repeated the experiment and analyzed barcodes in the E, M, and B lineages at 4 months after transplantation of control or EPO-exposed HSCs (160 and 1,000 ng/ml) (Fig. 6). In the control group, as reported before[66], the chimerism at 4 months after transplantation was increased compared to one month post-transplantation and the number of barcodes detected in HSCs was lower than at the early timepoints after transplantation (Fig. 6c-d and 1b-d). We detected no significant changes in the clonal composition or clonal output of HSCs between control and EPO group at this timepoint, implying that the effect of direct EPO-exposure on HSCs is transient (Fig. 6a-b,e).

Discussion

We could establish here, that EPO does have a direct effect on HSC differentiation after transplantation. High output MEK-biased and MBDC-biased HSCs produced the majority (>60%) of mature hematopoietic cells after *in vitro* EPO exposure and transplantation. The increased erythroid-associated gene signature in a subset of HSCs after *in vitro* EPO-exposure suggests that EPO directly induced high output MEK-biased HSCs which is indirectly compensated for by occurrence of MBDC-biased HSCs to maintain a balanced production of hematopoietic cells. Our results are only partially in line with reports on the effect of high systemic EPO levels on HSC[17,19,18,20,16], implying that EPO-induced effects on the HSC niche might also influence HSC differentiation. The direct effect of EPO on HSCs we described here could be one of the factors underlying the development of adverse side effects and co-morbidities during long-term EPO use in the clinics. The effect of cytokines on HSCs has previously been suggested to consist of selective induction of proliferation in a pre-existing lineage-biased HSC subset, and a *de novo* lineage instruction[45,46,47,48,16]. Our results highlight a more complex picture with changes in HSC differentiation apparent at the single cell level, while masked at the bulk level by compensation and feedback mechanisms.

Materials and methods

Mice

Male C57BL/6J CD45.1^{+}, C57BL/6J CD45.2^{+}, and *Rosa26CreER^{T2};mT/mG* mice aged between 7-13 weeks were used in all experiments. All procedures were approved by the responsible national ethics committee (APAFIS#10955-201708171446318 v1).

Barcode library, barcode reference list and lentivirus production

A new barcode library, named LG2.2, was generated. Oligo DNA stretches of 180 bp including a 20 bp "N"-stretch were ordered. DsDNA was generated by 10 PCR rounds and cloned into the XhoI-EcoRI site of the lentiviral pRRL-CMV-GFP plasmid[67]. Subsequently ElectroMaxStbl4 cells were transformed, and approximately 16,000 colonies picked for amplification by Maxiprep. A colony PCR showed approximately 15% of barcode negative colonies which led to an estimated final diversity of 13,000 barcodes for the new LG2.2 library. To create a barcode reference list as in[49], the pool of barcode plasmids was PCR amplified twice in duplicate using the a three-step nested PCR described in the barcode PCR section below and sequenced using SR65bp on a HiSeq 2500 System (Illumina) in Rapid run mode. Sequencing results were filtered to discard PCR and sequencing errors[49]. Briefly, resulting read numbers were normalized between replicates, sequences present in both replicates were sorted by frequency and the cumulative read number determined. Barcode sequences that made up less than 92,5% of the cumulative read number were discarded. Furthermore, barcodes that were above 1,5-fold more prevalent in one replicate and the most abundant barcodes were discarded. The resulting barcode reference list is present in Supplementary Table 3. Lentivirus was produced by transfecting the barcode plasmids

and p8.9-QV and pVSVG into HEK293T cells in DMEM-Glutamax supplemented with 10% FCS (Gibco), 1% MEM NEAA, and 1% sodium pyruvate using Polyethyleneimine. Supernatant was 0,45 um filtered, concentrated by 1h30 ultracentrifugation at 31 000g and frozen at -80°C.

HSC isolation, barcoding, EPO treatment, and transplantation

Isolation and labeling of cells with the LG2.2 lentiviral barcoding library was performed as described for the lentiviral barcoding library in[49]. Briefly, bone marrow cells were isolated from femur, tibia and iliac bones by flushing using a 21G needle (Terumo), and C-Kit$^+$ cells enriched using anti-CD117 magnetic beads (Miltenyi) on the MACS column system (Miltenyi). Cells were stained for C-kit, Flt3, CD150, Sca-1 (Table 1) and with Propidium iodine (Sigma) at a concentration of 1:5,000 directly before sorting and HSCs (LSK Flt3$^-$ CD150$^+$) (Supplementary Fig. 1a) were sorted. HSCs were transduced with the lentiviral barcode library in StemSpanMedium SFEM (STEMCELL Technologies) supplemented with 50 ng/ml mSCF (STEMCELL Technologies) through 1,5 h of centrifugation at 300 g and 4,5 h incubation at 37°C in order to obtain 10% barcoded cells. After transduction, human recombinant EPO (Eprex, erythropoietin alpha, Janssen) at a final concentration of 1,000 or 160 ng/ml or PBS was added and cells incubated for 16 hours at 37°C. After the incubation, the cells were transplanted in 6 Gy sub-lethally irradiated recipient mice. Approximately 2,600 cells (Mean 2684 cells +/- 175 cells) were injected in the tail vein of each mouse. When indicated, cells were injected together with additional EPO (16,000 IU/kg) at the moment of transplantation.

Cell progeny isolation for barcode analysis

At 4 weeks, or 4 months after transplantation, spleen, and/or blood, and/or bones (femurs, tibias and ilia) were isolated for barcode analysis from recipient mice. Spleens were mashed using 100 µm cell strainer (Gibco) and separated into a $Ter119^+$ and $Ter119^-$ fractions using a biotinylated anti-Ter119 antibody (Table 1) and anti-biotinylated beads (Miltenyi) on the MACS column system (Miltenyi). Blood cells were also separated into a $Ter119^+$ and $Ter119^-$ fraction using the same protocol. For both spleen and blood, $Ter119^+$ cells were stained for Ter119 and CD44. $Ter119^-$ cells were stained for CD45.1 CD11b, CD11c, CD19, and if appropriate CD115, Siglec-F, and Ly6G (Table 1). Bone marrow cells were extracted by flushing of the bones using a 21G needle (Terumo) and enriched using anti-CD117 magnetic beads (Miltenyi) on the MACS column system (Miltenyi). The $ckit^-$ fraction was further separated into a $Ter119^+$ and $Ter119^-$ fractions using the same protocol as for splenic and blood cells. $C\text{-}Kit^+$ cells were stained for c-Kit, Flt3, CD150, Sca-1, and if appropriate CD41 (Table 1). Propidium iodine (Sigma) was added at a concentration of 1:5000 directly before sorting (spleen and bone) or sole flow cytometric analysis (blood). Analyzed and/or sorted populations in spleen and blood were $Ter119^-$ and viable donor ($CD45.1^+$ or Tom^+) barcoded (GFP^+) B-cells (B; $Ter119^-$ $CD19^+$), myeloid cells (M; $Ter119^-$ $CD19^-$ $CD11c^-$ $CD11b^+$), erythroid cells (E; $Ter119^+$ $CD44^+$), and when appropriate dendritic cells (DC; $Ter119^-$ $CD19^-$ $CD1b^-$ $CD11c^+$) (Supplementary Fig. 1b-d), and myeloid subsets ($Ter119^-$ $CD19^-$ $CD11c^-$ $CD11b^+$) macrophages (Ma; $CD115^-$ $Siglec\text{-}F^-$ $Ly6G^-$), eosinophils (Eo; $CD115^-$ $Siglec\text{-}F^+$ $Ly6G^-$), monocytes (Mo; $CD115^+$ cells), and neutrophils (Neu; $CD115^-$ $Siglec\text{-}F^-$ $Ly6G^+$) (Supplementary Fig. 4a). Analyzed and/or sorted populations in bone were HSCs (LSK $Flt3^-$ $CD150^+$) and MkP ($C\text{-}Kit^+$, $Sca\text{-}1^-$, $CD150^+$, $CD41^+$) (Supplementary Fig. 1a,d).

Lysis, barcode amplification and sequencing

Sorted cells were lysed in 40 µl Viagen Direct PCR Lysis Reagent (cell) (Euromedex) supplemented with 0,5 mg/ml Proteinase K Solution RNA grade (Invitrogen) in a thermic cycler: (55°C for 120 min, 85°C for 30 min, 95°C for 5 min, indefinite at 4°C). Samples were then split into two replicates, and a three-step nested PCR was performed to, in a first step amplify barcodes (primers top-LIB (5′TGCTGCCGTCAACTAGAACA-3′) and bot-LIB (5′GATCTCGAATCAGGCGCTTA-3′)), in a second step add unique 4 bp plate indices (forward 5'ACACTCTTTCCCTACACGACGCTCTTCCGATCTNNNNCTAGAACACTCGAGAT CAG3′ and reverse 5'GTGACTGGAGTTCAGACGTGTGCTCTTCCGATCGATCTCGAATCAGGCGCTTA 3′), and in a third step add P5 and P7 flow cell attachment sequences and one of 96 sample indices of 7 bp P5 5'AATGATACGGCGACCACCGAGATCTACACTCTTTCCCTACACGACGCTCTTCC GATCT3′ and P7 5'CAAGCAGAAGACGGCATACGAGANNNNNNNGTGACTGGAGTTCAGACGTGCT CTTCCGATC3′) (PCR program: hot start 5 min 95°C, 15 s at 95°C; 30 s at 57.2°C; 30 s at 72°C, 5 min 72°C, 30 (PCR1-2) or 15 cycles (PCR 3)). Both index sequences (sample and plate) were designed based on[68] such that sequences differed by at least 2 bases, and homopolymers or more than 2 bp, hairpins and complementary regions with the rest of the primer sequence were absent (Supplementary Table 4 and 5). To avoid lack of diversity at the beginning of the reads during sequencing, at least 4 different plate indices were used for each sequencing run. Primers were ordered desalted, as high-performance liquid chromatography (HPLC) purified. During lysis and each PCR, a mock control was added. The DNA amplification by the three PCRs

was monitored by the run on a large 2% Agarose gel. Samples were pooled in order to guarantee a sequencing depth of 50 reads/cell. Five µl of the products of PCR3 for each sample and replicate were pooled, purified using the Agencourt AMPure XP system (Beckman Coulter), analyzed on a Bioanalyzer, and diluted to a concentration of 5 nM. These pools were sequenced on a HiSeq system (Illumina) (SR-65bp) at the sequencing facility of Institute Curie (10% of Phix Illumina phage genome library was added to generate a more diverse set of clusters).

Barcode sequence analysis

Sequencing results were analyzed using R-3.4.0 (R Development Core Team (2019) http://www.R-project.org.), Excel, and GraphPad Prism version 8.0 for Mac (GraphPad Software, La Jolla California USA, www.graphpad.com). Briefly, reads were first filtered for a 100% match in the input index- and common- sequences using XCALIBR (https://github.com/NKI-GCF/xcalibr) and filtered against the barcode reference list described above. Samples were filtered for containing at least 5000 reads and normalized to 10^5 per sample. Samples were then filtered for a Pearson correlation of barcodes above 90% between duplicates and reads present in only one of the two replicates were discarded. The mean of the replicates was used for further processing. As sometimes, the sharing of barcodes between mice was dependent on the sequencing runs rather than on the transduction batch, a filtering step was implemented as follows: When the mean percentage of barcodes shared between different sequencing runs was higher than within the same sequencing run for mice of a same transduction batch, reads below the read quartile of the mean percentage of barcodes shared between mice of a same transduction batch but sequenced on different sequencing runs were set to zero in order to equalize the barcode sharing between mice transplanted from a same transduction batch in different sequencing

runs to the barcode sharing between mice within each sequencing run. When indicated, heatmaps were generated using the R software on log10 transformed data using complete linkage and Euclidean distance (no reads are represented in black). When indicated, barcodes were categorized in progenitor classes either defining output in a lineage as presence of reads or using a previously published classifier[49]. In brief, read counts of each barcode in the different cell lineages were normalized enabling categorization into classes of biased output toward the analyzed lineages, using a threshold of 10% of a barcodes reads. Other thresholds were also analyzed (Supplementary Fig. 2c). Significance of changes in barcoding results (e.g. changed contribution of barcode classes to lineages) were analyzed using a permutation test as in[51]. Briefly, by permuting all mice of control and EPO groups, the generated differences of all random groupings were compared to the observed difference between control and EPO group. Significance of flow cytometry results was assessed using Student's T test when indicated.

ScRNAseq and analysis

ScRNAseq was performed using the 10x Genomics platform. Raw sequencing reads were processed using the 10x Genomics software Cellranger. To obtain a reads/cell/gene count table, reads were mapped to the mouse GRCm38.84 reference genome. scRNAseq analysis was performed using Seurat[59]. During filtering, Gm, Rik, and Rp genes were discarded as non-informative genes. Cells with less than 1,000 genes per cell and with a high percentage of mitochondrial genes were removed from downstream analyses. Data normalization was performed using the default Seurat approach and differentially expressed genes were determined using a logistic regression approach as implemented in Seurat. Unsupervised clustering was

performed on the significant variable genes using the ten first principle component analysis followed by the non-linear dimensionality reduction technique UMAP[69] (Supplementary Fig. 5b). We then performed unsupervised Louvain clustering of the data across a range of resolution parameters and chose the resolution value that led to the most stable clustering profiles[70] (Supplementary Fig. 5c). To identify EPO-responder cells in our EPO treated group, we first performed differential expression analysis between our control and treated groups. We then converted genes that were significantly (adjusted p-value< 0.05) upregulated in the EPO group into an EPO response signature which when overlaid onto our UMAP based visualization was enriched only in a subset of the EPO treated group cells. Cells in the upper 90th percentile with regards the expression of the EPO response signature were labelled EPO responders. To perform supervised cell type annotation, we generated a reference map from a published single cell sequencing dataset of 44,802 C-Kit^{+} cells processed using the 10X Genomics platform[55]. Data was downloaded from (https://github.com/theislab/paga) and preprocessed using an existing scanpy pipeline[57]. Data was then visualized using the non-linear non-dimensionality reduction technique UMAP[69]. We then map our cells onto this dataset using a k-nearest neighbors mapping approach. Briefly, for each cell in our query dataset we determine the nearest neighbors in PCA space of the reference dataset using the nn2 function of the RANN package[58] and take the mean UMAP 1 and 2 coordinates of the 10 nearest neighbors as the reference point for the new cell of interest. To benchmark the method, we used cells from an independent dataset of early erythroid progenitors and committed erythroid progenitors (cell type definitions are provided in the original publication) generated by[19] (data downloaded from https://kleintools.hms.harvard.edu/paper_websites/tusi_et_al/), no additional pre-

processing was performed before we aligned to our reference map and compared against known markers (Supplementary Fig. 5a,b).

Fluorescence activated cell sorting

FACS was performed at the flow cytometry facility of Institute Curie on a FACSAria™ (BD Biosciences). FACSDiva™ software (BD Biosciences) was used for measurements. Data analysis was performed using FlowJo™ v.10 (TreeStar). Cells were sorted using a 70 μm nozzle at precision 0/16/0 and high efficiency.

Data and script accessibility

All codes and data will be made available before publication on the github account of the Perié lab and ScRNAseq data will be deposited in the Gene Expression Omnibus (GEO) repository.

Author contributions

A.S.E designed experiments, performed experiments, and analyzed data; A.M, E.T and S.T.B performed experiments; T.T performed experiments and advised experiment design; J.C performed scRNAseq analysis with the feedback from A.M.L; J.U designed and made the lentiviral library under supervision; F.C produced the lentiviral library DNA stock; L.P designed experiment, advised data analysis and supervised the study; A.S.E and L.P wrote the paper, incorporating feedback from all coauthors.

Acknowledgements

We thank Dr. T. Schumacher for discussion and lentiviral library production and Dr. K Duffy for advices on permutation testing. We thank the Institute Curie flow cytometry, next generation sequencing, and animal facility. We thank Fahima Di Federico from the UMR168 BMBC facility for amplifying the barcode plasmid pool. A.S.E was supported by the IC-3i International PhD program of Institut Curie, in part funded by the European Commission´s MSCA COFUND scheme under the Marie Sklodowska-Curie Grant Agreement No 666003, and the Frontières de l´Innovation en Recherche et Education (FIRE) doctoral school of the Centre for Interdisciplinary research (CRI) Paris (Ecole doctroale n° 474, former Frontières du Vivants). The study was supported by an ATIP-Avenir grant from CNRS and Bettencourt-Schueller Foundation (to L.P.) and two grants from the *Labex CelTisPhyBio* ***(ANR-11-LABX-0038)*** and Idex Paris-Science-Lettres Program (ANR-10-IDEX-0001-02 PSL) (to L.P.). It was also supported by a starting ERC grant from the H2020 program (758170-Microbar to L.P.).

Competing interests statement

The authors declare no competing interests.

References

1. Sender, R., Fuchs, S. & Milo, R. Are We Really Vastly Outnumbered? Revisiting the Ratio of Bacterial to Host Cells in Humans. *Cell* **164**, 337–40 (2016).
2. Richmond, T. D., Chohan, M. & Barber, D. L. Turning cells red: signal transduction mediated by erythropoietin. *Trends Cell Biol.* **15**, 146–155 (2005).
3. Walsh, G. Biopharmaceutical benchmarks 2014. *Nat. Biotechnol.* **32**, 992–1000 (2014).
4. Koury, M. J. Tracking erythroid progenitor cells in times of need and times of plenty. *Exp. Hematol.* **44**, 653–63 (2016).
5. Pradeep, S. *et al.* Erythropoietin Stimulates Tumor Growth via EphB4. *Cancer Cell* **28**, 610–622 (2015).
6. Cheung Tung Shing, K. S. *et al.* EPO does not promote interaction between the erythropoietin and beta-common receptors. *Sci. Rep.* **8**, 12457 (2018).
7. Yang, F. *et al.* Cloning and characterization of a novel intracellular protein p48.2 that negatively regulates cell cycle progression. *Int. J. Biochem. Cell Biol.* **41**, 2240–50 (2009).
8. Li, C. *et al.* Erythropoietin Promotes Bone Formation through EphrinB2/EphB4 Signaling. *J. Dent. Res.* **94**, 455–463 (2015).
9. Singbrant, S. *et al.* Erythropoietin couples erythropoiesis, B-lymphopoiesis, and bone homeostasis within the bone marrow microenvironment. *Blood* **117**, (2011).
10. Ito, T., Hamazaki, Y., Takaori-Kondo, A. & Minato, N. Bone Marrow Endothelial Cells Induce Immature and Mature B Cell Egress in Response to Erythropoietin. *Cell Struct. Funct.* **42**, 149–157 (2017).
11. American Society of Hematology, S., Alvarez, J. C. & Noguchi, C. T. *Blood. Blood* vol. 130 (American Society of Hematology, 2017).
12. Zhang, Y. *et al.* Erythropoietin action in stress response, tissue maintenance and metabolism. *Int. J. Mol. Sci.* **15**, 10296–333 (2014).
13. Shiozawa, Y. *et al.* Erythropoietin Couples Hematopoiesis with Bone Formation. *PLoS One* **5**, e10853 (2010).
14. Tari, K. *et al.* Erythropoietin induces production of hepatocyte growth factor from bone marrow mesenchymal stem cells in vitro. *Biologicals* **45**, 15–19 (2017).
15. Cheshier, S. H., Prohaska, S. S. & Weissman, I. L. The effect of bleeding on hematopoietic stem cell cycling and self-renewal. *Stem Cells Dev.* **16**, 707–17 (2007).
16. Grover, A. *et al.* Erythropoietin guides multipotent hematopoietic progenitor cells toward an erythroid fate. *J. Exp. Med.* **211**, 181–188 (2014).
17. Giladi, A. *et al.* Single-cell characterization of haematopoietic progenitors and their trajectories in homeostasis and perturbed haematopoiesis. *Nat. Cell Biol.* 1 (2018) doi:10.1038/s41556-018-0121-4.
18. Yang, J. *et al.* Single cell transcriptomics reveals unanticipated features of early hematopoietic precursors. *Nucleic Acids Res.* **45**, 1281–1296 (2017).
19. Tusi, B. K. *et al.* Population snapshots predict early haematopoietic and erythroid hierarchies. *Nature* **555**, 54–60 (2018).

20. Singh, R. P. *et al.* Hematopoietic Stem Cells but Not Multipotent Progenitors Drive Erythropoiesis during Chronic Erythroid Stress in EPO Transgenic Mice. *Stem Cell Reports* **10**, 1908–1919 (2018).
21. Dubart, A. *et al.* Murine pluripotent hematopoietic progenitors constitutively expressing a normal erythropoietin receptor proliferate in response to erythropoietin without preferential erythroid cell differentiation. *Mol. Cell. Biol.* **14**, 4834–42 (1994).
22. Akashi, K., Traver, D., Miyamoto, T. & Weissman, I. L. A clonogenic common myeloid progenitor that gives rise to all myeloid lineages. *Nature* **404**, 193–197 (2000).
23. de Graaf, C. A. *et al.* Haemopedia: An Expression Atlas of Murine Hematopoietic Cells. *Stem cell reports* **7**, 571–82 (2016).
24. Forsberg, E. C., Serwold, T., Kogan, S., Weissman, I. L. & Passegué, E. New evidence supporting megakaryocyte-erythrocyte potential of flk2/flt3+ multipotent hematopoietic progenitors. *Cell* **126**, 415–26 (2006).
25. Mooney, C., Cunningham, A., Tsapogas, P., Toellner, K.-M. & Brown, G. Selective Expression of Flt3 within the Mouse Hematopoietic Stem Cell Compartment. *Int. J. Mol. Sci.* **18**, 1037 (2017).
26. Suszynska, M. *et al.* Expression of the erythropoietin receptor by germline-derived cells - further support for a potential developmental link between the germline and hematopoiesis. *J. Ovarian Res.* **7**, 66 (2014).
27. Wang, Z. *et al.* Receptor tyrosine kinase, EphB4 (HTK), accelerates differentiation of select human hematopoietic cells. *Blood* **99**, 2740–7 (2002).
28. Bennett, B. D. *et al.* Cloning and characterization of HTK, a novel transmembrane tyrosine kinase of the EPH subfamily. *J. Biol. Chem.* **269**, 14211–14218 (1994).
29. Suenobu, S. *et al.* A role of EphB4 receptor and its ligand, ephrin-B2, in erythropoiesis. *Biochem. Biophys. Res. Commun.* **293**, 1124–1131 (2002).
30. Baldridge, M. T., King, K. Y. & Goodell, M. A. Inflammatory signals regulate hematopoietic stem cells. *Trends Immunol.* **32**, 57–65 (2011).
31. Borghesi, L. Hematopoiesis in Steady-State versus Stress: Self-Renewal, Lineage Fate Choice, and the Conversion of Danger Signals into Cytokine Signals in Hematopoietic Stem Cells. *J. Immunol.* **193**, 2053–2058 (2014).
32. Metcalf, D. Hematopoietic cytokines. *Blood* vol. 111 485–491 (2008).
33. Sarrazin, S. & Sieweke, M. Integration of cytokine and transcription factor signals in hematopoietic stem cell commitment. *Seminars in Immunology* vol. 23 326–334 (2011).
34. Zhao, J. L. *et al.* Conversion of danger signals into cytokine signals by hematopoietic stem and progenitor cells for regulation of stress-induced hematopoiesis. *Cell Stem Cell* **14**, 445–59 (2014).
35. Endele, M., Etzrodt, M. & Schroeder, T. Instruction of hematopoietic lineage choice by cytokine signaling. *Exp. Cell Res.* **329**, 207–213 (2014).
36. Prendergast, Á. M. *et al.* IFN α -mediated remodeling of endothelial cells in the bone marrow niche. *Haematologica* **102**, 445–453 (2017).
37. Dykstra, B. *et al.* Long-Term Propagation of Distinct Hematopoietic Differentiation Programs In Vivo. *Cell Stem Cell* **1**, 218–229 (2007).
38. Morita, Y., Ema, H. & Nakauchi, H. Heterogeneity and hierarchy within the most primitive hematopoietic stem cell compartment. *J. Exp. Med.* (2010).
39. Oguro, H., Ding, L. & Morrison, S. J. SLAM family markers resolve functionally distinct subpopulations of hematopoietic stem cells and multipotent

progenitors. *Cell Stem Cell* **13**, 102–16 (2013).
40. Sanjuan-Pla, A. *et al.* Platelet-biased stem cells reside at the apex of the haematopoietic stem-cell hierarchy. *Nature* **502**, 232–6 (2013).
41. Carrelha, J. *et al.* Hierarchically related lineage-restricted fates of multipotent haematopoietic stem cells. *Nature* **554**, 106–111 (2018).
42. Yamamoto, R. *et al.* Clonal analysis unveils self-renewing lineage-restricted progenitors generated directly from hematopoietic stem cells. *Cell* **154**, 1112–26 (2013).
43. Lu, R., Neff, N. F., Quake, S. R. & Weissman, I. L. Tracking single hematopoietic stem cells in vivo using high-throughput sequencing in conjunction with viral genetic barcoding. *Nat. Biotechnol.* **29**, 928–33 (2011).
44. Verovskaya, E. *et al.* Heterogeneity of young and aged murine hematopoietic stem cells revealed by quantitative clonal analysis using cellular barcoding. *Blood* **122**, 523–532 (2013).
45. Matatall, K. A., Shen, C. C., Challen, G. A. & King, K. Y. Type II interferon promotes differentiation of myeloid-biased hematopoietic stem cells. *Stem Cells* **32**, 3023–3030 (2014).
46. Challen, G. A., Boles, N. C., Chambers, S. M. & Goodell, M. A. Distinct hematopoietic stem cell subtypes are differentially regulated by TGF-beta1. *Cell Stem Cell* **6**, 265–78 (2010).
47. Mossadegh-Keller, N. *et al.* M-CSF instructs myeloid lineage fate in single haematopoietic stem cells. *Nature* **497**, 239–243 (2013).
48. Etzrodt, M. *et al.* Inflammatory signals directly instruct PU.1 in HSCs via TNF. *Blood* **133**, 816–819 (2019).
49. Naik, S. H. *et al.* Diverse and heritable lineage imprinting of early haematopoietic progenitors. *Nature* **496**, 229–232 (2013).
50. Perié, L., Duffy, K. R., Kok, L., de Boer, R. J. & Schumacher, T. N. The Branching Point in Erythro-Myeloid Differentiation. *Cell* **163**, 1655–62 (2015).
51. Tak, T. *et al.* Simultaneous tracking of division and differentiation from individual hematopoietic stem and progenitor cells reveals within-family homogeneity despite population heterogeneity. *bioRxiv* 586354 (2019) doi:10.1101/586354.
52. Rodriguez-Fraticelli, A. E. *et al.* Clonal analysis of lineage fate in native haematopoiesis. *Nat. Publ. Gr.* **553**, (2018).
53. Theurl, I. *et al.* On-demand erythrocyte disposal and iron recycling requires transient macrophages in the liver. *Nat. Med.* **22**, 945–51 (2016).
54. Matsuoka, Y. *et al.* Low level of C-kit expression marks deeply quiescent murine hematopoietic stem cells. *Stem Cells* **29**, 1783–1791 (2011).
55. Dahlin, J. S. *et al.* A single-cell hematopoietic landscape resolves 8 lineage trajectories and defects in Kit mutant mice. *Blood* **131**, e1–e11 (2018).
56. Pietras, E. M. *et al.* Functionally Distinct Subsets of Lineage-Biased Multipotent Progenitors Control Blood Production in Normal and Regenerative Conditions. *Cell Stem Cell* **17**, 35–46 (2015).
57. Wolf, F. A. *et al.* PAGA: graph abstraction reconciles clustering with trajectory inference through a topology preserving map of single cells. *Genome Biol.* (2019) doi:10.1186/s13059-019-1663-x.
58. RANN: Fast Nearest Neighbour Search (Wraps ANN Library) Using L2 Metric version 2.6.1 from CRAN.
59. Satija, R., Farrell, J. A., Gennert, D., Schier, A. F. & Regev, A. Spatial reconstruction of single-cell gene expression data. *Nat. Biotechnol.* **33**, 495–

502 (2015).
60. Starnes, L. M. *et al.* NFI-A directs the fate of hematopoietic progenitors to the erythroid or granulocytic lineage and controls β-globin and G-CSF receptor expression. *Blood* **114**, 1753–1763 (2009).
61. Meenhuis, A. *et al.* MiR-17/20/93/106 promote hematopoietic cell expansion by targeting sequestosome 1-regulated pathways in mice. *Blood* **118**, 916–925 (2011).
62. Blank, U. *et al.* Smad7 promotes self-renewal of hematopoietic stem cells. *Blood* (2006) doi:10.1182/blood-2006-02-005611.
63. Steffen, B. *et al.* AML1/ETO induces self-renewal in hematopoietic progenitor cells via the Groucho-related amino-terminal AES protein. *Blood* **117**, 4328–4337 (2011).
64. Kim, S. *et al.* Dynamics of HSPC repopulation in nonhuman primates revealed by a decade-long clonal-tracking study. *Cell Stem Cell* (2014) doi:10.1016/j.stem.2013.12.012.
65. Aiuti, A. *et al.* Lentiviral hematopoietic stem cell gene therapy in patients with wiskott-aldrich syndrome. *Science (80-.).* **341**, (2013).
66. Wu, C. *et al.* Geographic clonal tracking in macaques provides insights into HSPC migration and differentiation. *J. Exp. Med.* **215**, 217–232 (2018).
67. Dull, T. *et al.* A Third-Generation Lentivirus Vector with a Conditional Packaging System. *J. Virol.* **72**, 8463 (1998).
68. Faircloth, B. C. & Glenn, T. C. Not All Sequence Tags Are Created Equal: Designing and Validating Sequence Identification Tags Robust to Indels. *PLoS One* **7**, e42543 (2012).
69. McInnes, L., Healy, J., Saul, N. & Großberger, L. UMAP: Uniform Manifold Approximation and Projection. *J. Open Source Softw.* (2018) doi:10.21105/joss.00861.
70. Blondel, V. D., Guillaume, J. L., Lambiotte, R. & Lefebvre, E. Fast unfolding of communities in large networks. *J. Stat. Mech. Theory Exp.* (2008) doi:10.1088/1742-5468/2008/10/P10008.

Figure legends

Fig. 1: High output ME- and MB-biased HSCs occur after transplantation of EPO-exposed HSCs. **a**, HSCs were sorted from the bone marrow of donor mice, lentivirally barcoded and cultured *in vitro* with or without 1,000 ng/ml EPO for 16h and transplanted into sublethal-irradiated mice. At week 4 post-transplantation, the erythroid (E), myeloid (M), and B-cells (B) lineages were sorted from the spleen and processed for barcode analysis. **b**, The percentage of donor derived cells ($CD45.1^+$) among the total spleen, myeloid cells ($CD11b^+$) or B-cells ($CD19^+$) in the spleen of control and EPO group. **c**, To better assess chimerism in erythroid cells mTdTomato/mGFP donor mice were used. The fraction of Tom^+ cells among erythroid cells ($Ter119^+$) in the spleen and blood in control and EPO group. **d**, Number of barcodes retrieved in the indicated lineages at week 4 after transplantation in control

and EPO group. **e**, Triangle plots showing the relative abundance of barcodes (circles) in the E, M, and B lineage with respect to the summed output over the three lineages (size of the circles) for control and EPO group. **f**, Percentage of HSCs classified by the indicated lineage bias, using a 10% threshold for categorization. **g**, Quantitative contribution of the classes as in f to each lineage. Shown are values from several animals (n= 8 EPO, n= 10 control in b, n= 3 EPO, n=4 control in c spleen, n= 4 EPO, n=8 control in c blood collected over 5 different experiments (d-g) n=5 for control and n=2 for EPO group collected over one experiment). For all bar graphs mean and S.D. between mice are depicted. Statistical significance tested using Student-T-test p=0,05 for (b-c).

Fig. 2: Effect of different EPO concentrations on clonality after HSC transplantation. Same protocol as in Fig. 1 but HSCs were cultured with different concentrations of EPO (160 ng/ml or 1,000 ng/ml) for 16 h, and when indicated a single dose of EPO (16,000 IU/kg) was injected together with barcoded HSCs at the moment of transplantation. **a**, Triangle plots showing the relative abundance of barcodes (circles) in the erythroid (E), myeloid (M), and B-lymphoid (B) lineage with respect to the summed output over the three lineages (size of the circles) for the different experimental groups as indicated. Shown is data pooled from several mice. **b**, The percentage of each lineage produced by the barcodes categorized by bias using a 10% threshold. Shown are mean and S.D. between mice (n=2 for 160 ng/ml, 1,000 ng/ml, and 160 ng/ml + EPO injection, n=4 for 1,000 ng/ml + EPO injection (collected over 4 different experiments)).

Fig. 3: Production of Dendritic Cells (DC) and Megakaryocyte Progenitors (MkP) by HSC after EPO-exposure and transplantation. In addition to the analysis of barcodes in the erythroid (E), the myeloid (M), and the B-cell (B) lineage, the DC lineage in spleen and MkP in bone marrow were added. **a**, Percentage of barcoded HSCs producing DC in the different HSC categories (classification as in Fig. 2 based on the M, E, and B lineage only using a 10% threshold. The DC only category was added). **b**, The percentage of the DC lineage produced by the barcodes categorized by bias as in a. **c-d**, Representations as in a-b for barcode detection in MkP. Data is derived from a cohort with detailed myeloid sorting. The myeloid lineage was merged according to the percentage of total donor myeloid as in Supplementary Fig. 4a to allow

classification as in a-b based on the M, E, and B lineage only using a 10% threshold. The MkP only category was added. Shown are values from several animals (a-b, n=5 for control and n=2 for EPO group, c-d, n=3 for control and n=1 for EPO group (collected over two experiments)). For all bar graphs mean and S.D. between mice are depicted.

Fig. 4: EPO exposed HSC characterization by scRNAseq. a, Overview of the reference map using supervised cell type annotation of the dataset from[55]. **b**, HSCs were sorted, barcoded and cultured in vitro with or without 1,000 ng/ml EPO for 16h, and analysed by scRNAseq using the 10X Genomics platform. Mapping of the transcriptomes of the 1,706 cells from control and 1,595 cells from EPO group obtained after quality control onto the reference map using a k-nearest neighbors mapping approach. **c**, Volcano plot of log2 fold change of the differentially expressed genes between control and EPO-exposed cells versus the adjusted p-value. Genes of interest are annotated. The significantly upregulated genes were used to defined a EPO-response signature. **d**, UMAP visualization of the EPO treated and control HSCs. **e**, The level of expression in the EPO exposed HSCs of the genes in the EPO-response signature (top), and definition of the EPO responder and EPO non-responder subgroups using the 90th percentile expression of the EPO-response signature from c (bottom). **f**, The expression of the indicated genes in the control, EPO responder and EPO non-responder subgroups as defined in e. Statistical comparisons were made using a one-way ANOVA with p-values adjusted for multiple comparisons using Dunnett´s multiple comparison test.

Fig. 5: Overlap of barcodes in HSCs and mature cells after transplantation of EPO-exposed HSCs. Same protocol as in Fig. 1 but HSCs were cultured with two different concentrations of EPO (160 ng/ml or 1000 ng/ml) for 16h. In addition, HSCs were sorted and subjected to barcode analysis. **a**, The total number of barcodes found back in HSCs. **b**, The percentage of barcodes in the mature cell subsets also detected in HSCs and the percentage of barcodes in HSCs also detected in mature cells. **c**, The percentage of the HSC lineage contributed by barcodes categorized by bias as in Fig. 2 based on the M, E, and B lineage using a 10% threshold. **d**, The percentage of each lineage produced by the barcodes color coded for presence (blue) and absence (grey) in HSCs. Shown are values from several animals (n=5 for control, n=2 for EPO 160

ng/ml group and n=3 for EPO 1,000 ng/ml group. For all bar graphs mean and S.D. between mice are depicted.

Fig. 6: The effect of EPO on HSC clonality after transplantation is transient. Same protocol as in Fig. 2, but barcodes in the E, M, and B lineage in spleen of individual mice sacrificed at month 4 post-transplantation were analyzed. **a**, Triangle plots showing the relative abundance of barcodes (circles) in the erythroid (E), myeloid (M), and B-cell (B) lineage with respect to the summed output over the three lineages (size of the circles) for the different experimental groups as indicated. **b**, Quantitative contribution to each lineage of the HSC classes that were classified using a 10% threshold. **c**, The fraction of donor cells among the indicated cell types in spleen. **d**, Barcode number retrieved in the indicated lineage at month 4 after transplantation in control (black dot), EPO 160 ng/ml (red square), and EPO 1,000 ng/ml (red triangle) group. **e**, Proportion of HSCs classified using a threshold of 10% in experimental groups as indicated. Shown are data pooled from several mice. (**c**, n=5 for control and n=4 for each EPO group, (a-b, d-e) n=6 for control and n=4 for each EPO group (collected over two experiments). For all bar graphs mean and S.D. between mice are depicted.

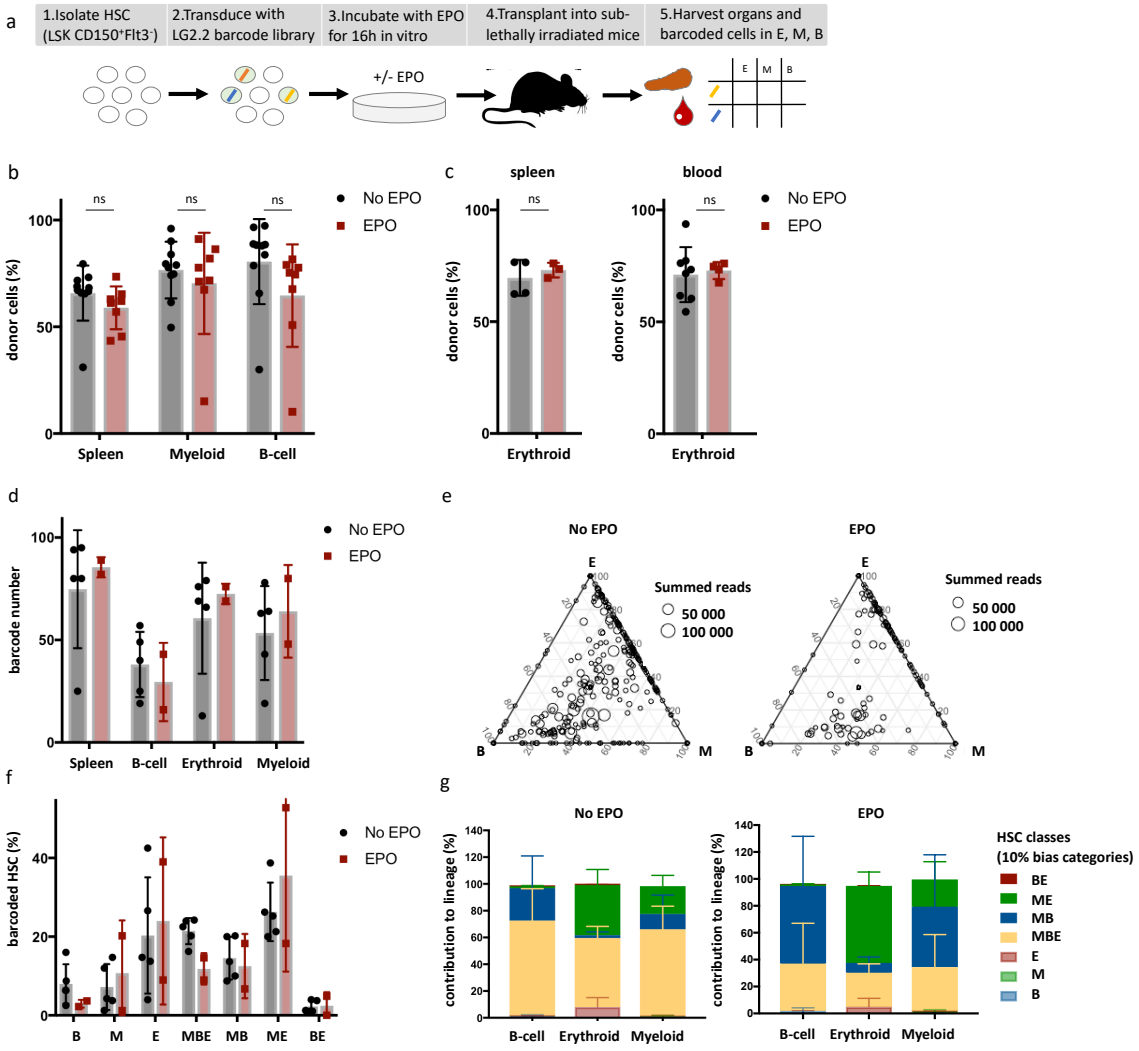

Fig. 1

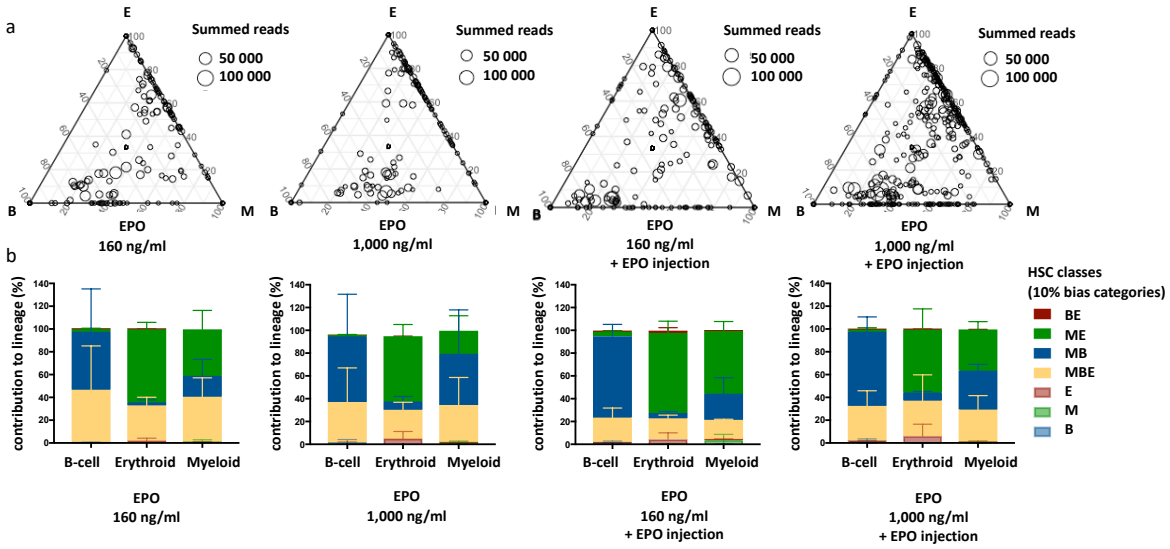

Fig.2

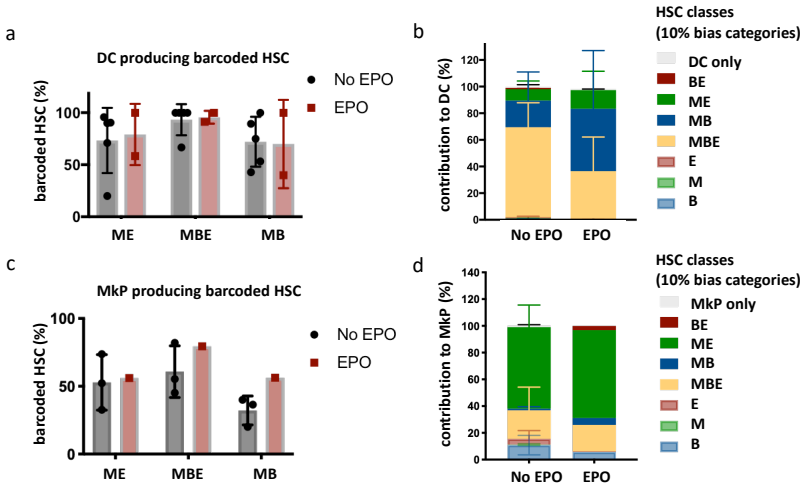

Fig. 3

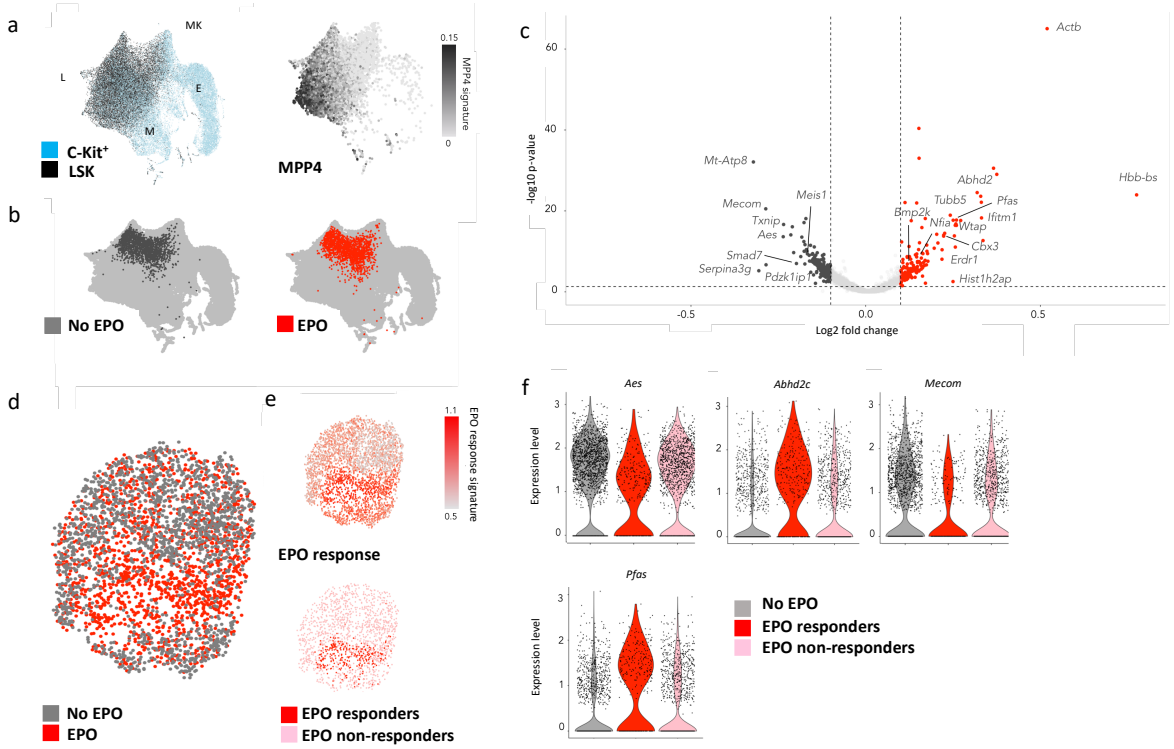

Fig. 4

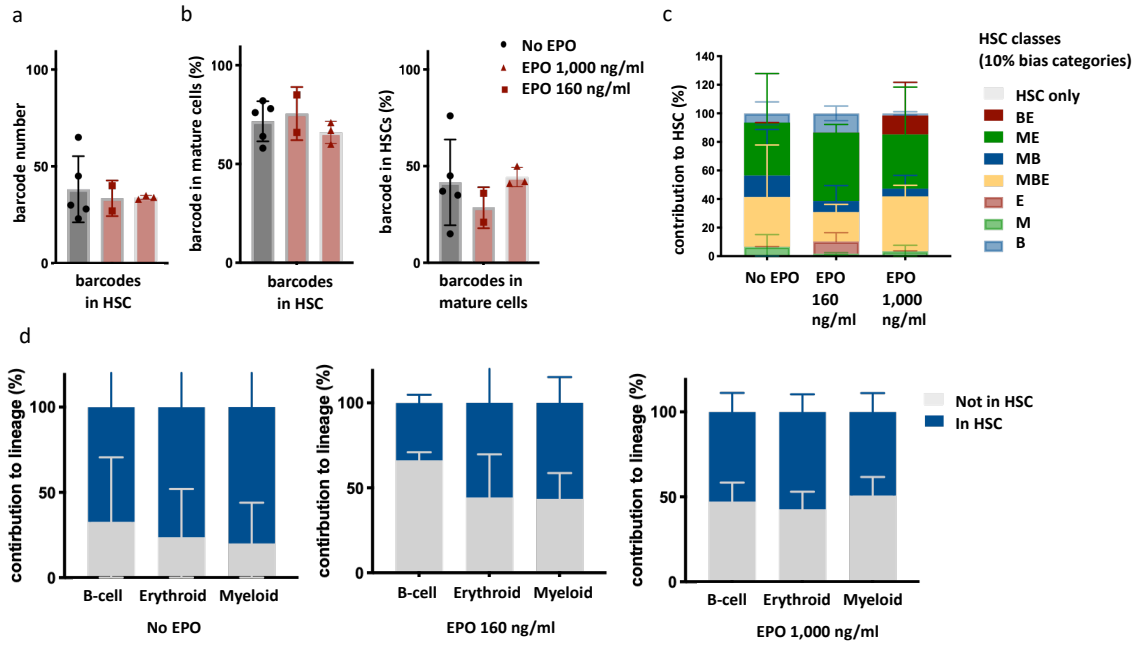

Fig. 5

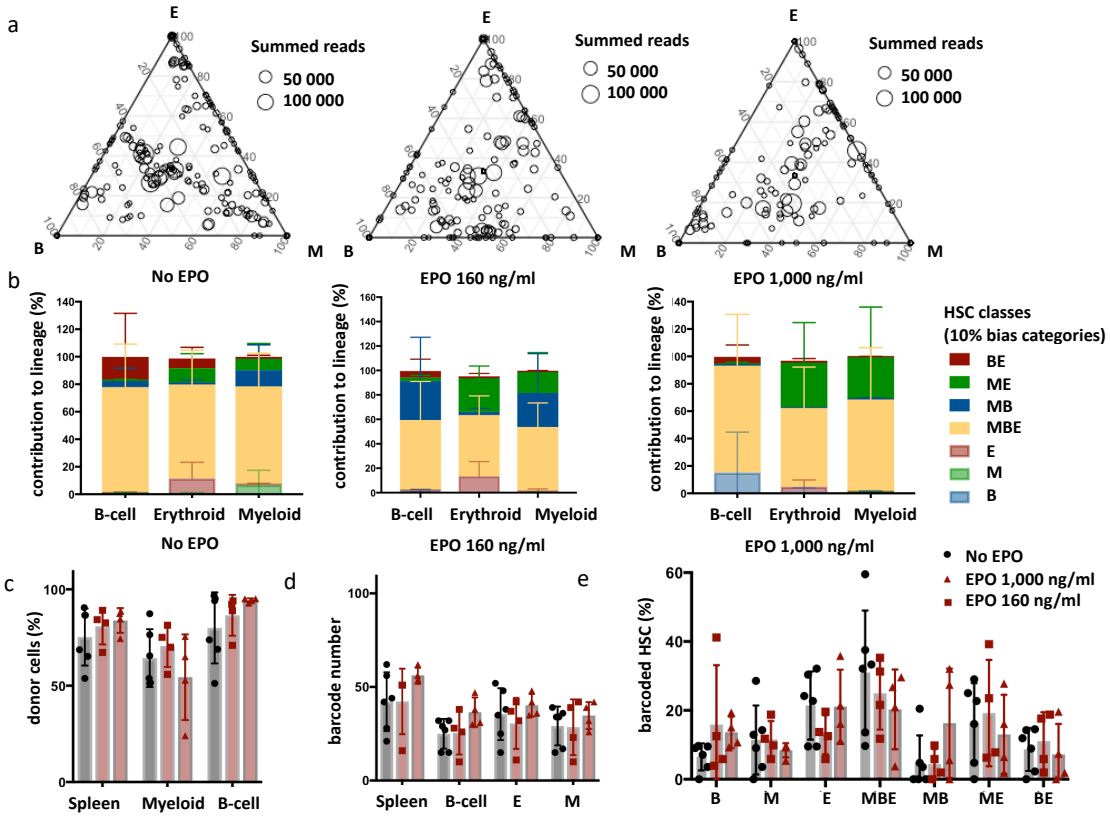

Fig. 6

Tables

Table 1: Fluorescently labeled antibodies

Antibody target	Clone	Conjugate	Manufacturer
CD45.1	A20	PE	BD Biosciences
Ter119	TER119	PE-Cy7	BD Biosciences
CD11c	N418	APC	eBioscience
CD19	1D3	APC-Cy7	BD Biosciences
CD11b	M1/70	PerCP-Cy5.5	eBioscience
CD117 (C-Kit)	2B8	APC	BioLegend
CD135 (Flt3)	A2F10	PE	eBioscience
CD135 (Flt3)	A2F10	PE-Cy5	Life technologies
Sca1	D7	Pacific Blue	BioLegend
CD150	TC15-12F12.2	PE-Cy7	BioLegend
Ter119	TER119	biotin	BD Biosciences
CD44	IM7	PE	BD Biosciences
CD41	MVVREG30	BV510	BD Biosciences
Siglec-F	E50-2440	PE-CF594	BD biosciences
Ly6G	1A8	BV510	BioLegend
CD115	AFS98	PE	BioLegend